RESEARCH ARTICLE
doi: 10.2306/scienceasia1513-1874.2025.004

ScienceAsia 51 (1): 2025: ID 2025004: **1–7**

Microscopic and spectroscopic investigation of deposited thin opal films using an electric field assisted capillary deposition method

Muhammad Engki Saputra[a], **Mulda Muldarisnur**[a,*], **Frank Marlow**[b], **Dahyunir Dahlan**[a]

[a] Department of Physics, Faculty of Mathematics and Natural Sciences, Universitas Andalas, Padang 25163 Indonesia
[b] Max Planck Institut für Kohlenforschung, 45470 Mülheim an der Ruhr, Germany

*Corresponding author, e-mail: muldarisnur@sci.unand.ac.id

Received 31 Oct 2023, Accepted 4 Nov 2024
Available online 15 Feb 2025

ABSTRACT: Despite being a preferred approach for fabricating three-dimensional photonic crystals, self-assembly of colloidal particles is indispensably restricted by internal defects. External fields like electric fields may provide more controlled self-assembly by tuning colloidal particles' movement, aggregation, and ordering processes. This research aimed to improve the quality of opal films deposited using the capillary deposition method by applying a direct current (DC) electric field. DC electric field of 150 V/cm was applied to planar cells to influence self-assembly. We varied the relative orientation of gravitation and Coulomb force by depositing opal at an inclined angle of $0° \leqslant \alpha \leqslant 90°$ with steps of 15°. This inclination corresponds to the parallel and perpendicular orientation of these forces. Microscopic and spectroscopic investigations revealed convincing influences of inclination angle on crystal domain size and optical properties of the resulting opal films. The largest average crystal domain area of 138 mm^2 and the most homogeneous opalescent films were obtained for an inclination angle of 45°. Maximum absorbance, background, and Bragg peak width also appeared at an inclination angle of 45°. This work shows the possibility of improving opal film quality using a DC electric field.

KEYWORDS: opal films, capillary deposition method, DC electric field, inclination angle, defect

INTRODUCTION

All-optical data processing is the most anticipated component for developing high-speed data transmission in communication and information technology. Photonic crystals have paved the way to control photon propagation and emission, enabling the fabrication of many optical devices [1]. Photonic crystals are artificial structures having a periodic variation in their refractive indices on the scale of the optical wavelengths. Most polychromatic electromagnetic waves that enter photonic crystals will propagate without any disruption, except for those whose wavelengths fall between a specific range known as the photonic band gap (PBG), where light propagation is not allowed. These frequencies of electromagnetic waves induce destructive interference inside photonic crystals; hence the surface of the photonic crystal will reflect them. Owing to the probability of creating PBG, it would be possible to manipulate the propagation of light [2]. Photonic crystals may be ideal for manipulating light propagation and interaction with matter. Photonic crystals have been reported for various applications, such as beam splitters [3], waveguides [4], sensors [5], nanocavity lasers [6], superlenses [7], and many others.

Self-assembly is a promising (low-cost and straightforward) approach for fabricating 3D photonic crystals [8]. It can be used over a vast range (i.e., from nanometer to micrometer scale [9]) of colloidal particle sizes, therefore beneficial for adjusting the PBG position required for intended applications [10]. Self-assembly results in structures consisting of ordered colloidal particles, called opals, containing internal defects in the form of point defects, stacking faults, domains, thickness inhomogeneities, and cracks. Defects creates allowed states in the PBG due to the disruption in the periodicity that may lead to band gap closing when defect concentration is too high. The existence of internal defects limits the applicability of opals in optical devices [11]. Many self-assembly methods are available, for example, sedimentation [12], horizontal deposition [13], vertical deposition [14], and capillary deposition [15]. Sedimentation is the simplest but results in disordered particle arrangement for large particles and is time-consuming for small particles. The quality of opals deposited using horizontal deposition, or vertical deposition, method is much improved but depends on many deposition parameters that have yet to be fully understood. Despite having unintended defects, the capillary deposition method (CDM) results in high opal quality, as indicated by the observation of high-order diffraction peaks [16–18] and oriented domains [19]. The formation mechanism of CDM-made opal films has also been quite well understood [20, 21].

A more directed particle movement, aggregation, ordering, and growth using external fields may help reduce opals' defect contents. An electric field is a

better alternative than other external fields because it can be used for almost all types of colloidal particles in suspension due to the possession of surface charges obtained via selective adsorption or desorption. DC electric field has been used in many methods including sedimentation [22], horizontal deposition [23], vertical deposition [24], and capillary deposition [25, 26].

In order to increase the ordering quality of resulting opals, the slow (fast) sedimentation rate for small (diameter less than 200 nm) and large (diameter above 500 nm) particles was adjusted using an electric field. Increased domain size and better ordering quality have been reported, but an ordering quality gradient over opal film thickness was also apparent [27]. Applying an electric field in the vertical deposition method showed quicker deposition of thick opal films with enhanced particle ordering and bigger domain sizes. Random hexagonal close-packing particle arrangement and thickness fluctuation along the growth direction are unavoidable despite some improvements. A DC electric field for opal deposition using the CDM method has been applied. The planar cell used for the opal deposition was aligned horizontally so that gravity and electrostatic forces were either parallel or antiparallel. The optimum voltage obtained is 1.5 V for opal films of 50 µm thick, i.e., equivalent to an electric field of 300 V/cm when the gravity and electrostatic force are in the opposite direction [25]. In another work, we found that an electric field of 80 V/cm is optimum for electrostatic force perpendicular to gravity [26]. The parallel orientation of electrostatic force and gravity results in low-quality opal films.

It is, therefore, fascinating to know how the relative orientation of the electrostatic and gravity forces affects the structure of the resulting opals. In addition to affecting colloidal particle movement, gravity plays a substantial role in the adsorption of sub-micrometer-sized particles on a solid substrate [28]. Gravity determines the surface arrangement of colloidal particle aggregates or nuclei during deposition at the growth front. In this work, we used the CDM to deposit opal films with a constant electric field by varying the planar cell's inclination angle. The inclination allows variation in the relative orientation between gravity and electrostatic forces that influence the structure and optical properties of the resulting opal films.

MATERIALS AND METHODS

Suspension of polystyrene nanoparticles (250 nm in diameter) was purchased from Microparticles GmbH (Berlin, Germany) and used without any treatment except dilution. Before opal preparation, the original 10 wt% suspension was diluted in bi-distilled water to obtain 1 wt% suspension. After dilution, the suspension bottle was placed in an ultrasonic bath for 30 min to ensure the diluted suspension's homogeneity. Polystyrene nanoparticles were used in this work instead of silica or poly-methyl methacrylate because of their easy-to-synthesize and modify nature. The refractive index of polystyrene is also higher; it is beneficial to obtain a wider band gap.

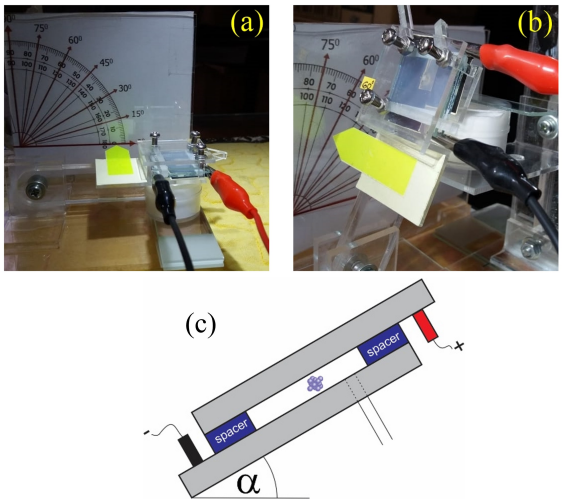

Fig. 1 Electric field assisted capillary deposition method for different inclination angle: (a), 0°; (b), 60°; and (c), the scheme of planar capillary cell connected with positive and negative terminals of power supply.

Planar cell assembly

A planar capillary cell, consisting of two glass substrates, was used to deposit an opal film in the CDM. To enable electric field application, square indium tin oxide (ITO)-coated glass slides (25 mm × 25 mm) from Sigma-Aldrich (distributed by New Praktika Alkesindo, Jakarta, Indonesia) were used as substrates to build the planar cell (see Fig. 1). A 1-mm hole was drilled in one of the substrates at a distance of 5 mm from an edge. During the cleaning procedure, substrates were inserted in a staining jar and placed in an ultrasonic bath (Ultrasonic 600 ml, Krisbow, Indonesia). Acetone (Bratachem, Tangerang, Indonesia), isopropyl alcohol (Bratachem), and bi-distilled water were poured into and removed sequentially from the staining jar for 10 min while ultrasonicated. Clean substrates were stored in a clean staining jar filled with bi-distilled water. Clean substrates in the staining jar were dried using a hair dryer before use. A capillary tube (18 mm long) was inserted into the drilled hole and then glued using an epoxy resin. Two polymer spacers (25 mm × 3 mm) with a thickness of 50 µm, defining the thickness of the resulting opal film, were placed onto the second glass slide without a hole using tweezers. The substrates were sandwiched with the conductive parts facing each other, and then the planar cell was wrapped using Parafilm. The horizontal position of the substrates was shifted slightly to enable

contact with power supply terminals.

Opal deposition

A DC power supply (PS-305D, Kenika, Indonesia) generated a homogeneous electric field inside the planar capillary cell during the deposition process. The voltage difference generated by the power supply was kept constant at 0.75 V, an optimal voltage based on our previous work [25]. Zero voltage results in slightly polycrystalline samples where hexagonal and rectangular colloidal particle arrangements were observed in some areas. Then, the planar cell was placed on a homemade inclined stage. The positive and negative terminals were connected to the ITO substrates using crocodile clips (Fig. 1), where the negative terminal was connected to the bottom substrate. Negative bottom substrate results in better opal quality [25]. Immediately after the capillary tube was immersed in the suspension container, the suspension was lifted into the planar cell due to the generated capillary force in the tube and then by steady solvent evaporation at the open edges. Continuous solvent evaporation allows steady opal growth along the open edges, where particles accumulate and crystallize [10]. The inclination angle of the planar cell (α) was set in the range of $0^\circ \leqslant \alpha \leqslant 90^\circ$ with steps of 15°. Opal deposition was followed by recording an image every 10 min using a HAYEAR Camera (Shenzhen Hayear Electronics, Shenzen, China).

Sample characterization

In this work, we focused on macroscopic defects, namely domains, and cracks whose size is larger than the unit cell of colloidal crystals [29]. The quality of deposited opal was first evaluated using direct visual observation. Opals with good quality show homogeneous opalescence over a large sample area. Opal films were characterized using an optical microscope (CX-23 LED RF, Olympus, Tokyo, Japan) and UV/vis Spectrometer (Genesys 840-208100, Thermo Scientific, Massachusetts, USA). The optical surface roughness of samples was inferred from the opalescent homogeneity of recorded opal images analyzed using ImageJ™ software. Crack distance and domain size were measured using the optical microscope. The scale bar of the microscope was obtained by taking a picture using an objective lens with a predefined ruler on it. The crack distance and domain size were averaged over more than 20 measurements.

RESULTS AND DISCUSSION

Structure of opal films

At the beginning of this research, the DC voltage was set at 1.5 V, following our previous work [25]. Opals deposited at inclination angles of 0° and 15° grew as expected. A different result was found for the sample deposited at an inclination of 30°. When the voltage difference of 1.5 V was applied, electrolysis of suspension inside the planar cell was observed (Fig. S1). Hydrogen and oxygen were formed from the electrolytic process on the surface of the ITO substrates at this voltage, combined with more accessible gas release from the substrate to inhibit particle ordering and growth. As a result, opaque and non-homogeneously distributed particle aggregation was obtained. Once trapped gas was formed, opal growth was no longer possible. Likely, the electrolysis also occurred at low inclination angles (0° or 15°), but the static microbubbles self-blocked the electrolysis. Only the mobility of the bubbles allowed the process to go on. In any case, the process was not useful for the deposition process. We then decided to reduce the voltage to 0.75 V or an electric field of 150 V/cm, which was then used to prepare all reported samples. No significant differences between opal formation at different inclination angles, and no solvent electrolysis was observed.

An optical microscope was used to observe the formed photonic crystal domains (Fig. 2(a–c)). Parallel-oriented cracks perpendicular to opal drying fronts were observed in most of the sample area. Network-type cracks were observed near open edges and formed uncracked domains. Parallel cracks in the CDM-made opals were formed due to directional drying front oriented parallel to the open edges. Cracks were formed at the open edges and then propagate into the middle of the sample area.

For further analysis of domain size, we divided the area of opal film in the planar cell into three sections: left, center, and right, to make it easier to see the distribution of the crystal domains. Each section was divided into two groups, as shown in Fig. 2(e). The calculated average domain size of each sample (using ImageJ™ software) was displayed in Fig. 2(d). The average domain sizes of the left (area 1 + area 6) and the right sections (area 3 + area 4) were nearly similar, i.e., within the measurement uncertainty, except for an inclination angle of 30°. The center region (area 2 + area 5) consistently had a larger average uncracked domain size. A larger domain was caused by an elongated and widened domain shape close to the capillary tube that was not observed in the other sections. Network-type cracks near planar cell edges were formed due to rapid solvent evaporation soon after sample detachment from the suspension container, forming smaller domains. Planar cells with an inclination angle of 45° had the largest centre area of 1.38 mm^2. The measured area was three orders of magnitude larger than the reported values in the literature, which is about 500 μm^2. However, the most important aspect of Fig. 2 was likely that the sample was inhomogeneous in its defect distribution.

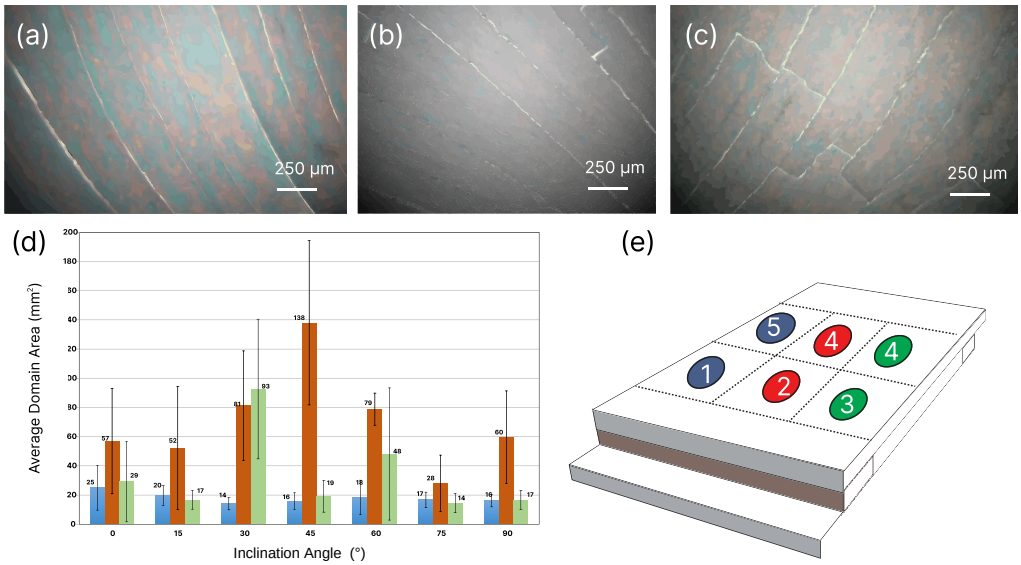

Fig. 2 Optical microscope images of opal films deposited at different angles: (a), 0°; (b), 45°; and (c), 90°; (d), calculated average domain size in different analysis sections (color code as in Fig. 2e); and (e), analysis sections at the planar cell.

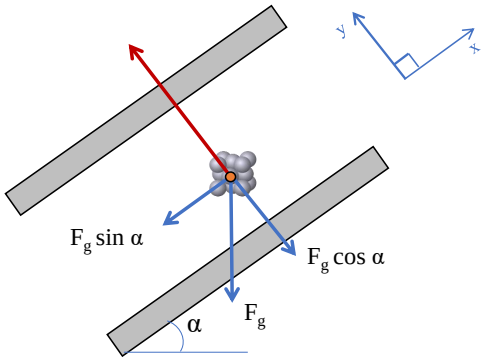

Fig. 3 Forces acting on colloidal particle aggregates inside the planar capillary cell, with the capillary forces pointing outward (inward) the paper, parallel to the open edges.

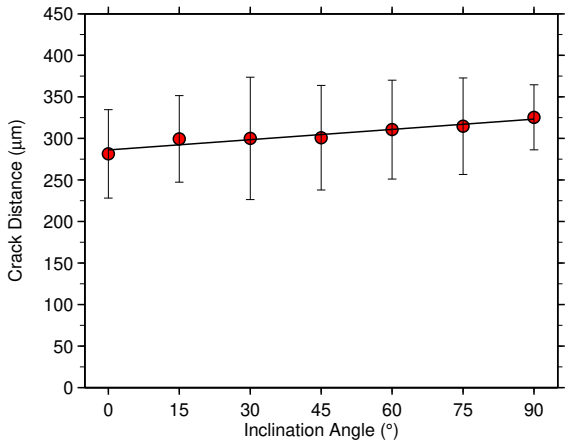

Fig. 4 Average distance between neighboring cracks as a function of inclination angle of planar cell.

This surprising result could be due to the fact that the growth direction was changing over the sample, as visible in Fig. 1(d), showing a bent growth front. We would try to enhance this effect in future experiments, extending the conditions for regions 2 and 5 for larger parts of the sample.

Fig. 3 shows a description of forces acting on the planar cell during opal synthesis. The capillary force was parallel to the inclined plane toward the open edges. The electrostatic force was perpendicular to the substrate (i.e., normal to the planar cell), whereas the gravity formed an angle with respect to the substrate. The cosine projection of gravitational force was anti-parallel to the electrostatic force, while the sine projection was perpendicular to the electrostatic force and the capillary force. Opal film started to grow from the open edges inward into the center of the planar capillary cell. The magnitudes of DC voltage and crystal thickness were constant, so the Coulomb or electrostatic force in the planar cell was the same for all samples. Capillary forces lifted the colloidal particle suspension into the planar cell before spreading in all directions to fill the cell. Charged particles underwent electrophoretic movement when an electric field was applied due to its interaction with an electric double

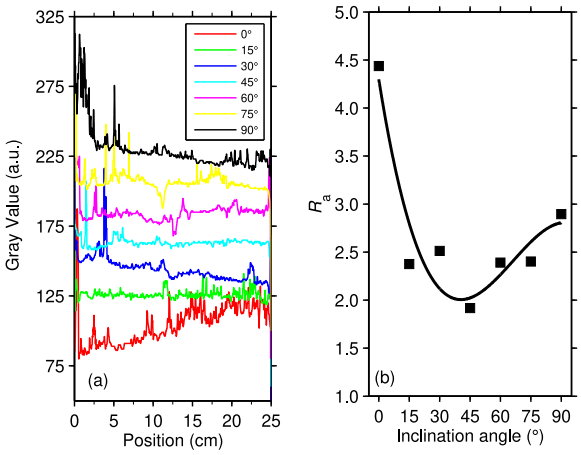

Fig. 5 (a), Surface roughness of opal thin films at different inclination angles (note: gray value between data for consecutive inclination angles were shifted by 20 to enhance visibility); and (b), average roughness (R_a) value of opals.

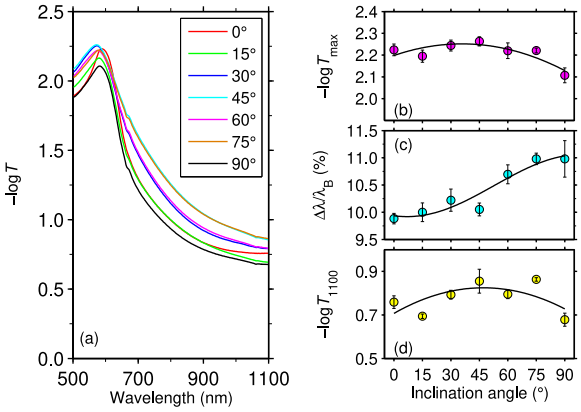

Fig. 6 (a), Spectra of thin opal films; (b), absorbance; (c), normalized FWHM; and (d), background or absorbance at 1100 nm of thin opal films.

layer on the surface of particles. When negatively charged ions from the dispersion medium adhered to the surface of colloidal particles, the particles acquired a negative electric charge; and, hence, resulting in the negative particle drawing in positive counterions nearby. The electric double layer refers to the area around a dispersed phase particle, encompassing the ions attached to the particle's surface and a layer of the dispersion medium with the opposite charge. The potential at the electric double layer determines interactions between colloidal particles and with external electric field [30].

The Coulomb force is always perpendicular to the opal growth front (open edges of the planar cell). The Coulomb force is antiparallel with the gravity at an inclination angle of 0° and becomes perpendicular at an angle of 90°. Gravity is much weaker than Coulomb force for single particles but becomes comparable for particle aggregates or colloidal crystal nuclei [24]. A negative terminal on the bottom substrates was chosen to avoid rapid sedimentation, resulting in low-quality opal films. Stable colloidal crystal growth is achieved when the Coulomb force has the same magnitude as the capillary forces. By projecting the gravitational force of particle aggregate and then assuming a stable opal growth, one obtains the equilibrium when $\tan\alpha = 1$ or the inclination angle of 45°. In this argument, large crystal domains are formed when the ordering quality is improved because cracks are normally formed at the domain boundaries. Larger domains imply better opal quality.

An optical microscope was used to measure the distance of the neighbouring cracks in opals. Cracks are common phenomena on drying objects like colloidal suspensions or thin films. Cracks are formed due to unbalanced shrinkage of opal films and substrate; therefore, they are challenging to avoid for films deposited on solid substrates. The average crack distance of the opal as a function of the inclination angle was shown in Fig. 4. The cracks in CDM-made opals deposited under the influence of the electric field were nearly parallel to each other, similar to the crack alignment for conventional CDM-made opals. The distance between neighbouring cracks depends on thickness [19, 31, 32]. In this work, however, the opal film thickness was kept constant at 50 µm. Based on our previous work, the film thickness was exactly the same as the spacer thickness, and the thickness gradient had never been observed. Therefore, the variation of crack distance must be related to the inclination angle. The crack distance only slightly linearly (0.5 nm/degree slope) increased with the inclination angle. A larger inclination angle changed the force balance so that the projection of the gravity parallel to the substrate increased. The increase might cause compaction or densification of the colloidal crystals, causing an increase in average crack distance. The average crack distance was around 325 µm, much higher than the reported value in previous research, which was 110–155 µm [33–35]. A larger crack distance could be due to a much higher humidity during drying than the cited works.

ImageJ™ software was used to evaluate the opalescent homogeneity of the resulting opals. The average opalescent roughness (R_a) did not show actual spatial roughness. Instead, it showed the roughness in opalescent or optical properties. We converted recorded colour images of opal films into their gray value data to calculate roughness parameters, namely R_a, the most commonly used surface texture parameter. The R_a value indicates the average surface roughness across the sample surface, i.e., the average difference between peaks and valleys. The greater the

deviations are, the rougher the surface will be; and if the R_a value is small, the surface is smooth. The surface roughness of opal films at different angles could be seen in Fig. 5(a). Fig. 5(b) shows the results of the R_a analysis. Opal deposited with a slope of 45° had the smallest R_a, implying it had the smoothest surface or the most homogeneous opalescence compared to other opals. Our result showed that the most homogeneous opal in terms of its opalescence was obtained for a deposition angle of 45°. This likely corresponded to better opal quality and large average uncracked domains.

Optical properties of opal films

Determination of opals' absorbance peak and maximum absorbance wavelength was carried out using a UV/Vis-NIR Spectrophotometer. Absorbance peaks indicate the presence of an optical band gap in opal thin films [16]. The wavelength used in the spectrophotometer was set in the range of 500–1100 nm. Each opal had one absorbance peak at a specific wavelength (Fig. 6). The opal transmission spectra consisted of a Bragg peak and a continuous background. The Bragg peak did not change strongly. However, the background spectra changed drastically. Here, the background was described by the extinction spectra ($E = -\log T$) at 1100 nm. This wavelength was chosen because it was far from the Bragg wavelength. The maximum absorbance value was in the range of 2.001–2.283, with the wavelength when maximum absorbance was 570–582 nm. The maximum extinction was equivalent to less than 1% transmission, indicating high penetration inhibition of light inside the opals. Non-zero transmission comes from scattering by defects [19, 34]. They will likely reduce significantly the maximum of $-\log T$ at the Bragg peak, as the cracks might allow a small fraction of the incident light to penetrate the samples. Maximum absorbance and narrow Bragg peak occurred at 45°, corresponding to the largest average domain size and the lowest opalescent inhomogeneity. These data indicated that high-quality opal films were obtained at an inclination angle of 45°. The normalized full width at half maximum (FWHM), the ratio of FWHM to the Bragg wavelength, tended to increase with angle. The increase might be caused by sedimentation of particle aggregates on the lower edge of the planar capillary cell. Slight variation in the background could be due to measurement uncertainty.

CONCLUSION

Our results showed the significance of planar cell orientation (i.e., inclination angle) for opal fabrication from colloidal suspensions and provided the possibility for controlling the quality of the opal films. Although detailed theoretical explanations of the observations could be complex, because of the complexity of the processes accompanying deposition, the available parameters could be used to explain them. The orientation of the planar cell played an essential role in the deposition of opal films from colloidal suspensions. The inclination angle determined the competition between capillarity and electrostatic forces, which occurred during the deposition process and determined the structural and optical properties of the final opal films. High-quality opal films with large domain areas have been successfully deposited by optimizing planar cell orientation under the electric field.

Appendix A. Supplementary data

Supplementary data associated with this article can be found at https://dx.doi.org/10.2306/scienceasia1513-1874.2025.004.

Acknowledgements: This work was supported by Universitas Andalas with research Grant No. T/40/UN16.19/PT.01.03/IS-RPT/2023.

REFERENCES

1. Rehman AU, Khan Y, Irfan M, Butt MA (2023) Investigation of optical-switching mechanism using guided mode resonances. *Photonics* **10**, 13.
2. Butt MA, Khonina SN, Kazanskiy NL (2021) Recent advances in photonic crystal optical devices: a review. *Opt Laser Technol* **142**, 107265.
3. Wang J, Pei L, Weng S, Wu L, Huang L, Ning T, Li J (2017) A tunable polarization beam splitter based on magnetic fluids-filled dual-core photonic crystal fiber. *IEEE Photonics J* **9**, 2200410.
4. Dutta HS, Goyal AK, Srivastava V, Pal S (2016) Coupling light in photonic crystal waveguides: a review. *Photonics Nanostructures: Fundam Appl* **20**, 41–58.
5. De M, Gangopadhyay TK, Singh VK (2019) Prospects of photonic crystal fiber as physical sensor: an overview. *Sensors* **19**, 464.
6. Ota Y, Katsumi R, Watanabe K, Iwamoto S, Arakawa Y (2018) Topological photonic crystal nanocavity laser. *Commun Phys* **1**, 86.
7. Zheng G, Xie A, Xu L, Lai M, Wu Y, Liu Y (2015) Point imaging through one-dimensional graded metal-dielectric photonic crystals. *Optik* **126**, 400-402.
8. Cai Z, Li Z, Ravaine S, He M, Song Y, Yin Y, Zheng H, Teng J, et al (2021) From colloidal particles to photonic crystals: advances in self-assembly and their emerging applications. *Chem Soc Rev* **50**, 5898–5951.
9. Schyck S, Meijer J-M, Baldauf L, Schall P, Petukhov AV, Rossi L (2022) Self-assembly of colloidal superballs under spherical confinement of a drying droplet. *JCIS Open* **5**, 100037.
10. Tahami SHV, Pourmahdian S, Hadavand BS, Azizi ZS, Tehranchi MM (2016) Termal tuning the reversible optical band gap of self-assembled polystyrene photonic crystals. *Photonics Nanostructures: Fundam Appl* **22**, 40–45.
11. Marlow F, Muldarisnur M, Sharifi P, Brinkmann R, Mendive C (2009) Opals: status and prospects (invited review). Angew Chem Int Ed **48**, 22.
12. Li Y, Lan Z, Guojin L, Liqin C, Qinguo F, Jianzhong S (2018) Study on the fabrication of composite photonic crystals with high structural stability by co-

sedimentation self-assembly on fabric substrates. *Appl Surf Sci* **444**, 145–153.

13. Utgenannt A, Maspero R, Fortini A, Turner R, Florescu M, Jeynes C, Kanaras AG, Muskens OL, et al (2016) Fast assembly of gold nanoparticles in large-area 2D nanogrids using a one-step, near-infrared radiation-assisted evaporation process. *ACS Nano* **10**, 2232–2242.
14. Liu G, Zhou L, Wu Y, Wang C, Fan Q, Shao J (2015) The fabrication of full color P(St-MAA) photonic crystal structure on polyester fabrics by vertical deposition self-assembly. *J Appl Polym Sci* **132**, 41750.
15. Li H-L, Dong W, Bongard H-J, Marlow F (2005) Improved controllability of opal film growth using capillaries for the deposition process. *J Phys Chem B* **109**, 9939-9945.
16. Muldarisnur M, Popa I, Marlow F (2012) Angle-resolved transmission spectroscopy of opal films. *Phys Rev B* **86**, ID 8.
17. Muldarisnur M, Marlow F (2016) Polarization angular-resolved transmission spectroscopy of opal films. *JNOPM* **25**, 1650015.
18. Marlow F, Muldarisnur M, Sharifi P, Zabel H (2011) Interpretation of small-Angle diffraction experiments on opal-like photonic crystals. *Phys Rev B* **84**, ID 4.
19. Muldarisnur M, Marlow F (2011) Opal films made by the capillary deposition method: crystal orientation and defects. *J Phys Chem C* **115**, ID 5.
20. Muldarisnur M, Marlow F (2017) Spectroscopic investigation of opal formation from suspensions. *J Phys Chem C* **121**, 18274–18279.
21. Muldarisnur M, Marlow F (2014) Observation of nano-dewetting in colloidal crystal drying. *Angew Chem Int Ed* **53**, ID 5.
22. Rogach AL, Kotov N, Koktysh DS, Ostrander J, Ragoisha GA (2000) Electrophoretic deposition of latex-based 3D colloidal photonic crystals: a technique for rapid production of high-quality opals. *Chem Mater* **12**, 2721–2726.
23. Katagiri K, Tanaka Y, Uemura K, Inumaru K, Seki T, Takeoka Y (2017) Structural color coating films composed of an amorphous array of colloidal particles via electrophoretic deposition. *NPG Asia Mater* **9**, 355.
24. Napolskii KS, Sapoletova NA, Gorozhankin DF, Eliseev AA, Chernyshov DY, Byelov DV, Grigoryeva NA, Mistonov AA, et al (2010) Fabrication of artificial opals by electric-field-assisted vertical deposition. *Langmuir* **26**, 2346–2351.
25. Muldarisnur M, Marlow F (2022) Structure and optical properties of opal films made by an out-of-plane electric field-assisted capillary deposition method. *ACS Omega* **7**, 8084–8090.
26. Muldarisnur M, Marlow F (2023) Effect of an in-plane electric field on the formation and optical properties of opal films. *AIP Conf Proc* **2694**, 020011.
27. Holgado M, García-Santamaría F, Blanco A, Ibisate M, Cintas A, Míguez H, Serna CJ, Molpeceres C, et al (1999) Electrophoretic deposition to control artificial opal growth. *Langmuir* **15**, 4701–4704.
28. Diba FS, Boden A, Thissen H, Bhave M, Kingshott P, Wang P-Y (2018) Binary colloidal crystals (BCCs): Interactions, fabrication, and applications. *Adv Colloid Interface Sci* **261**, 102–127.
29. Yevchik A, Moiseyenko V, Dergachov M (2015) The influence of structural defects on the optical properties of synthetic opals. *Ukr J Phys Opt* **16**, 24–31.
30. Somphon W, Loisruangsin A (2023) ZIF-8, chitosan and β-cyclodextrin-incorporated ZIF-8 nanohybrid for improving drug delivery. *ScienceAsia* **49**, 776–785.
31. Lee WP, Routh AF (2004) Why do drying films crack? *Langmuir* **20**, 9885–9888.
32. Allain C, Limat L (1995) Regular patterns of cracks formed by directional drying of a collodial suspension. *Phys Rev Lett* **74**, 2981.
33. Hartsuiker A, Vos WL (2008) Structural properties of opals grown with vertical controlled drying. *Langmuir* **24**, 4670–4675.
34. Astratov VN, Adawi AM, Fricker S, Skolnick MS, Whittaker DM, Pusey PN (2002) Interplay of order and disorder in the optical properties of opal photonic crystals. *Phys Rev B* **66**, 165215.
35. Suh Y, Pham Q, Shao B, Won Y (2019) The control of colloidal grain boundaries through evaporative vertical self-assembly. *Small* **15**, 1804523.

Appendix A. Supplementary data

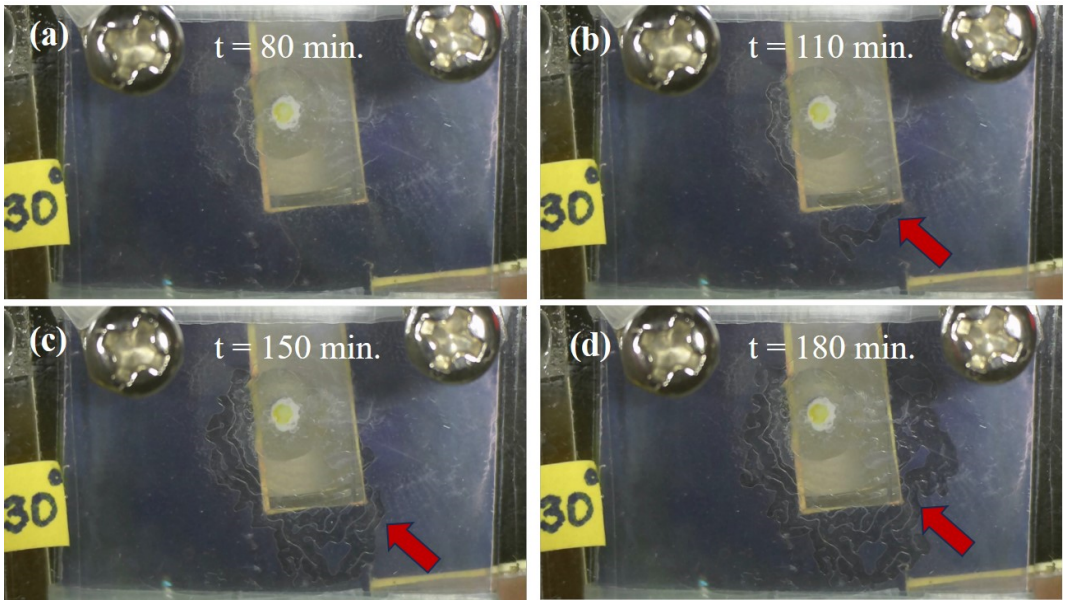

Fig. S1 Electrolysis in a planar cell with an inclination angle of 30° when a voltage of 1.5 V was applied: (a), before electrolysis, t = 80 min; (b), after electrolysis, t = 110 min; (c), after electrolysis, t = 150 min; (d), after electrolysis, t = 180 min. The arrows showed trapped gas produced by the electrolysis process. Black paper was placed underneath the planar cell to obtain better contrast. Bubble started to form near the capillary tube which then became larger until the deposition process had stopped by itself due to blocking of suspension supply.